J|A|C|S
ARTICLES
Published on Web 11/22/2002

Creating New Supramolecular Materials by Architecture of Three-Dimensional Nanocrystal Fiber Networks

Xiang Yang Liu,*,† Prashant D. Sawant,† Wee Beng Tan,‡ I. B. M. Noor,‡ C. Pramesti,‡ and B. H. Chen‡,§

Contribution from the Department of Physics, National University of Singapore, 2 Science Drive 3, Singapore 117542 and the Department of Chemical and Environmental Engineering, National University of Singapore, 10 Kent Ridge Crescent, Singapore 119260

Received April 29, 2002

Abstract: The architecture of three-dimensional interconnecting self-organized nanofiber networks from separate needlelike crystals of L-DHL (lanosta-8,24-dien-3β-ol:24,25-dihydrolanosterol = 56:44) in di-isooctylphthalate has been achieved for the first time, on the basis of the completely new concept of branching creation by additives (branching promoters). [In this work, an additive, ethylene/vinyl acetate copolymer (EVACP), is used at a concentration of several 10 ppm.] We demonstrate that this novel technique enables us to produce previously unknown self-supporting supramolecular functional materials with tailormade micro- or nanostructures, possessing significantly modified macroscopic properties, by utilizing materials thus far considered to be "useless". In addition, both the self-organized structure and the properties of the new materials can be fine-tuned by altering the processing conditions. Our results show that the formation of the interconnecting 3D self-organized network structure is controlled by a new mechanism, so-called crystallographic mismatch branching mechanism, as opposed to the conventionally adopted molecular self-assembly mechanism. The principles and criteria for the selection of branching promoters are also discussed from the point of view of molecular structures.

Introduction

Supramolecular functional materials[1] having 3D fibrous network structures formed by interconnecting nanosized fibers have important applications in drug delivery, coatings, lithography, catalyst supporters, scaffolds for tissue engineering, the engineering of nanosctructural materials and self-supporting porous materials in the novel separation for macromolecules, and so forth.[1−6] Macroscopic properties, in particular the rheological properties of supramolecular functional materials, are determined by the microstructure of fiber networks. Fibrous networks with permanent interconnections will effectively entrap and immobilize liquid in the meshes and possess both the elastic properties of ideal solids and the viscosity properties of Newtonian liquids, leading to the formation of self-supporting supramolecular materials.[2,4,7] In contrast, systems consisting of nonpermanent or transient interconnecting (or entangled) fibers or needles can only form weak and viscous paste at low concentrations.[2]

Since there is no sufficient understanding, significant efforts have been devoted to identify novel systems with the three-dimensional (3D) interconnecting self-organized network structure to obtain *such functional materials* with the desirable properties.[2,4,5] This includes the screening of a large number of compounds and solvents molecules, as well as suitable solvent capable of forming these structures.[2,4−6] In some cases, because of the limitation in the choice of materials, screening becomes impossible. On the other hand, if interconnecting 3D micro- or nanofiber networks with the required organization can be constructed, new functional materials with the required functionalities can be produced. Obviously, this is a completely new route in producing new functional materials.

We will in this paper report a completely new approach to produce new macromolecular functional materials by means of constructing 3D permanent interconnecting nanocrystal fibrous networks with tailormade micro- or nanostructure and expected properties from a system consisting of separate crystal needles (cf. Figure 1a) and to engineer the materials with required micro-

* Address correspondence to this author. E-mail: phyliuxy@nus.edu.sg.
† Department of Physics.
‡ Department of Chemical and Environmental Engineering.
§ Current address: Dept of Chem. Eng., National Cheng Kung University, 1 University Road, Tainan, Taiwan.

(1) (a) Mio, M, J.; Moore, J. S. *MRS Bull.* **2000**, *25*, 36−41. (b) Derossi, D.; Kajiwara, K.; Osada, Y.; Yamauchi, A. *Polymer Gels: Fundamentals and Biomedical Applications*; Plenum Press: New York, 1991. (c) Guenet, J. M.; *Thermoreversible Gelation of Polymers and Biopolymers*; Academic Press: London, 1992. (d) Corriu, R. J. R.; Leclercq, D. *Angew. Chem.* **1996**, *108*, l524−1540; (e) *Angew. Chem., Int. Ed Engl*. **1996**, *35*, 1420−1436. (f) Reetz, M. I. *Adv. Mater*. **1997**, *9*, 943−954.
(2) Terech, P.; Weiss, R. G. *Chem. Rev*. **1997**, *97*, 3133−3159.
(3) Brunsveld, L.; Folmer, B. J. B.; Meijer, E. W. *MRS Bull*. **2000**, *25*, 49−53.
(4) van Esch, J. H.; Feringa, B. L. *Angew Chem., Int. Ed*. **2000**, *39*, 2263−2266.
(5) Oya, T.; Enoki, T.; Grosberg, A. U.; Masamune, S.; Sakiyma, T.; Tekeoka, Y.; Tanaka, K.; Wang, G.; Tilmaz, Y.; FeId, M. S.; Dasari, R.; Tanaka, T. *Science* **1999**, *286*, 1543−1545.
(6) Terech, P.; Rodrigez, V.; Barnes, J. D.; Mckenna, G. D. *Langmuir* **1994**, *10*, 3406.
(7) Hiemenz, P. C.; Rajagopalan, R. *Principles of Colloid and Surface Chemistry*; Marcel Dekker: New York, 1997; p 145−192.

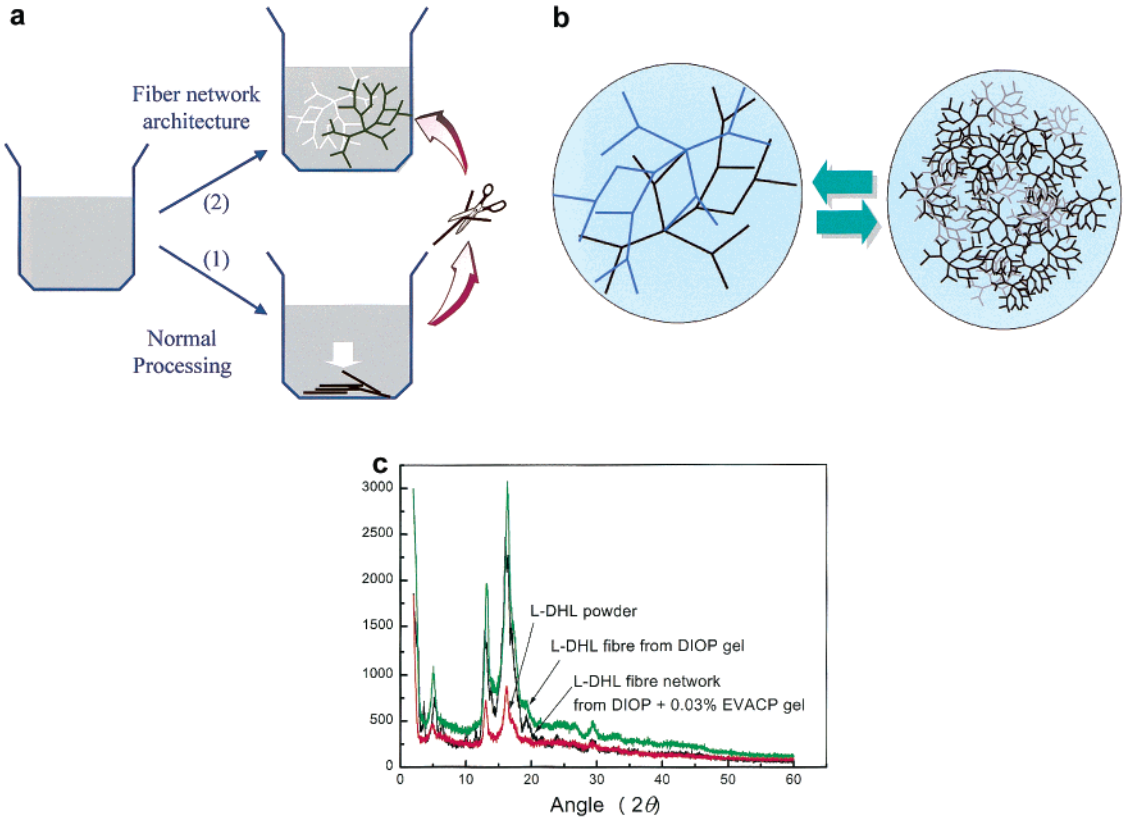

Figure 1. (a) and (b): Illustration of micro- or nanostructure engineering of functional materials. (a) Network architecture (route 2) with respect to normal fiber formation; (b) modification of micro- or nanostructure of 3D interconnecting fiber network. (c) X-ray diffraction analysis for L-DHL crystalline powders and fibers. They all reveal identical crystalline structures.

or nanostructure (Figure 1b), on the basis of a completely new network building mechanism.

Experimental Section

The materials to be examined were obtained by L-DHL (lanosta-8,24-dien-3β-ol:24,25-dihydrolanosterol = 56:44, from Sigma) in DIOP (di-(2-ethyl-hexyl) phthalate $(C_8H_{17}COO)_2$ C_6H_4 liquid) (99%, Cognis) at ~120 °C to form a L-DHL/DIOP solution and by lowering the sample temperature to a lower temperature (around room temperature), called the experimental temperature hereafter. A multiphase system or a supramolecular material was obtained when L-DHL precipitated out from the solution at that temperature. L-DHL powders used in our experiments are in a crystalline state (cf. the X-ray diffraction results in Figure 1c.)

To examine the nano- or microstructure of fibrous networks in supramolecular materials, scanning electronic microscope (SEM), coupled with a CO_2 supercritical fluid extraction technique (Thar Design), was applied. The purpose of implementing the latter is to remove the liquid captured in the networks without disturbing the essential structure of networks.[8]

To evaluate the impact of EVACP on the formation of the interconnecting 3D nanocrystal fiber networks on macroscopic properties of the materials, the rheological properties of the above system were measured by an advanced rheological expansion system (ARES-LS, Rheometric Scientific). The sample was subjected to sinusoidal oscillations by moving both the upper and the lower circular plates with a diameter of 25 mm (the gap between the two plates was 1.5 mm). The frequency was set to 0.1 Hz. Except the case shown in Figure 3b, the amplitude of the oscillations in our experiments was controlled to obtain a 0.1% strain in the sample. (Under this strain limit, the structure of the supramolecular materials will not be destroyed by the measurements.) The instantaneous measurement of the applied stress and the resultant strain allows the calculation of the storage modulus G' (describing the elastic property) and the loss modulus G'' (describing the viscosity property) and consequently the complex rnodulus G^* (= $[(G')^2 + (G')^2]^{1/2}$).[7,10−11]

Results and Discussion

Branching Creating and Micro/Nano Network Architecture. During the process of natural cooling of the aforementioned system (the concentration of L-DHL: 10 wt %) from 120 °C to room temperature (~20 °C), an opaque and viscous paste was obtained (see the right corner of Figure 2a). This SEM micrograph shows that the system consists of only separated L-DHL *needles* (short and thick fibers), which are in temporary contact with each other (see Figure 2a). This refers to the "normal processing" illustrated by Figure 1a.

To create networks with permanent interlinking from such a system as illustrated by route 2 in Figure 1a, an additive EVACP (ethylene/vinyl acetate copolymer, $(C_4H_6O_2)_x(C_2H_4)_y$, approximate MW ~ 100,000; from SP[2] Scientific Polymer Products Inc) was introduced to the identical L-DHL/DIOP solution as described above at 120 °C. The L-DHL/DIOP solution was cooled to the same experimental temperature under the identical conditions, to allow the occurrence of L-DHL in the liquid. It is surprising to see that the addition of a tiny amount of EVACP

(8) Ilzhoefer, J. R.; Spontak, R. J. *Langmuir* **1995**, *11*, 3288−3291.

(9) Meakin, P. *Phys. Rev. A* **1983**, *27*, 1495.
(10) Graff, D. S.; Sander, L. M. *Phys. Rev. E* **1993**, *47*, R2273.
(11) Van Cantfort, O.; Brasseur, A.; Michaux, B.; Pirard, R.; Pirard, J. P.; Lecloux, A. J. *Faraday Discuss.* **1995**, *101*, 265−274.

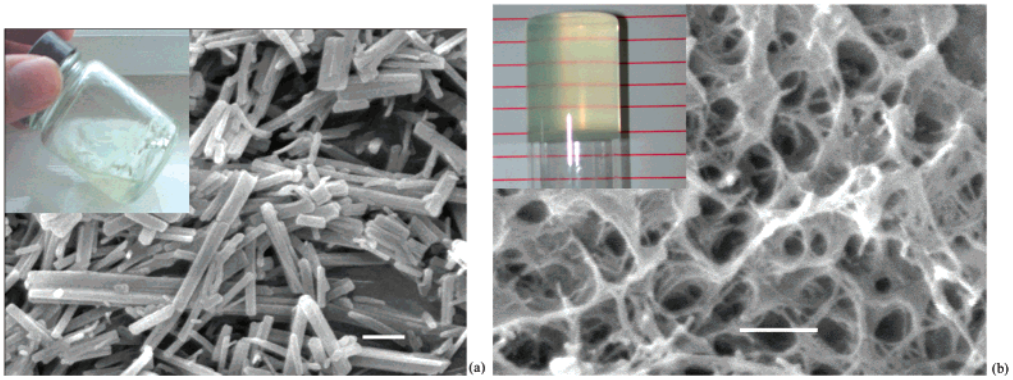

Figure 2. (a) Separate fibers occurring in the 10 wt % L-DHL/DIOP system. This system gives rise to an opaque as shown in the picture on the right upper corner. The length of the bar: 1 μm. (b) Interconnected fiber networks in 10 wt % L-DHL/DIOP system after adding 0.004 wt % EVACP. The length of the bar: 1 μm. This system gives rise to a clear and tough gel as shown in the picture on the right upper corner.

(0.004 wt %) is sufficient to create completely different micro/nano networks of interconnecting self-organized L-DHL nanocrystal fibers (Figure 2b) at the experimental temperature. This completely changes the rheological properties of the materials and leads to the formation of a self-supporting soft solidlike supramolecular material (see the upper corner of Figure 2b.)

Figure 3a shows the change of G^* as a function of time t for the L-DHL/DIOP system. G^* increases abruptly at $t \geq t_g$ (t_g: gelation time, cf. Figure 3a), indicating the formation of L-DHL crystalline fibers. G^* will reach its maximum value G^*_{max} as the formation of the fiber networks approaches completion at $t \rightarrow \infty$. In comparison with the controlled sample, G^*_{max} is almost doubled when a tiny amount of EVACP is added. (Similar changes were also obtained for G' and G''.)

Figure 3b shows the change of the storage modulus G' of the above system as a function of various oscillating strain amplitudes γ with angular frequency $\omega = 0.2\pi$ rad/sec. The strain corresponds to the deformation of the networks caused by the applied shear stress. G' remains constant (linear) at small strains and decreases abruptly when γ exceeds a certain value γ_o. The onset of the nonlinearity (decrease in G') at γ_o corresponds to the breakage of the junctions in the networks.[12] The result given in Figure 3b indicates that the addition of EVACP leads to a significant enhancement of the limit of linearity γ_o ($\sim$100 times cf. Figure 3b).

Figure 3a and b shows that a new macromolecular material with significantly modified macroscopic properties forms after the addition of EVACP. To the best of our knowledge, such a novel approach of creating new supramolecular materials by an additive has never been reported before.

The Mechanism of 3D Interlinking Network Formation. To explore the network promotion mechanism of EVACP, an adequate understanding on the cross-linking of fiber networks is required. The key issue to be addressed here is whether the formation of 3D interconnecting network of the small molecular organic gelling agents, such as L-DHL, is controlled by molecule self-assembly as suggested by most people.[4] It is extremely unlikely that the occurrence of a trace amount of EVACP will cause the lash-shape of L-DHL crystal needles as shown in Figure 2a to be assembled into the self-organized, regularly branched nanofiber networks as shown in Figure 2b.

As shown by the results of the X-ray diffraction (XRD) analysis in Figure 1b, L-DHL powders, needles, and 3D interconnecting fibers have identical crystalline structures. This implies that the formation of L-DHL needles and 3D interconnecting fibers is essentially controlled by a new kinetics associated with the nucleation-growth process. For the primary fiber formation, it should be controlled as most crystalline materials by a nucleation process, which can be verified by the linear relationship between $\ln t_g$ and $1/(\Delta\mu/kT)^2$[2,13−15] ($\Delta\mu$ denotes the chemical potential difference between L-DHL molecules in the fiber and in the liquid phase, k is Boltzmann's constant, T is temperature; to obtain $\Delta\mu/kT$, cf. eq 2).

According to 3D nucleation models, the nucleation rate J, the number of critical nuclei generated per unit time−volume at the substrate can be expressed as[13−15]

$$J = f'[f]^{1/2} B \exp\left[-\frac{16\pi\gamma^3_{cf}\Omega^2}{3(kT)^3[\Delta\mu/kT]^2} f\right] \qquad (1)$$

with

$$\frac{\Delta\mu}{kT} \cong \ln\left(\frac{X}{X_{eq}}\right) \qquad (2)$$

where Ω is the volume of growth units, γ_{cf} denotes the interfacial free energy of the tip of fibers and the fluid phase, B is kink kinetic coefficient and is constant for a given system, f and f' ($0 < f, f' \leq 1$) are the factors describing the correlation between the substrates and the nucleating phase,[13−15] and X and X_{eq} are the actual molar fraction and the equilibrium molar fraction of solute in solutions at a given temperature T, respectively. If the formation of fibrous networks is initiated by nucleation, one should have $t_g \sim 1/J$.[13] According to eq 1, for such a given system, we can then have a linear relationship between $\ln(t_g) \sim 1/(\Delta\mu/kT)^2$ for a given f. In Figure 4, the linear fits between $\ln(t_g)$ and $1/(\Delta\mu/kT)^2$ obtained for both the system without and with EVACP indeed verify this mechanism.

Referring to Figure 2b, it can be seen that one of the key steps in building up the self-organized interconnecting fiber

(12) Shih, W. H.; Shih, W. Y.; Kim, S. I.; Liu, J.; Aksay, I. *Phys. Rev. A* **1990**, *42*, 4772−4779.

(13) (a) Liu, X. Y. In *Advances in Crystal Growth Research*; Sato, K., Nakajima, K., Furukawa, Y., Eds.; Elsevier: Amsterdam, 2001; p 42−61. (b) Liu, X. Y. *J. Chem. Phys.* **2000**, *112*, 9949−9955.

(14) Liu, X. Y.; Sawant, P. D. *Appl. Phys. Lett.* **2001**, *79*, 3518−3520; *Adv. Mater.* **2002**, *14*, 421−426.

(15) Chernov, A. A. *Modern Grystallography III−Crystal Growth*; Springer-Verlag: Berlin, 1984.

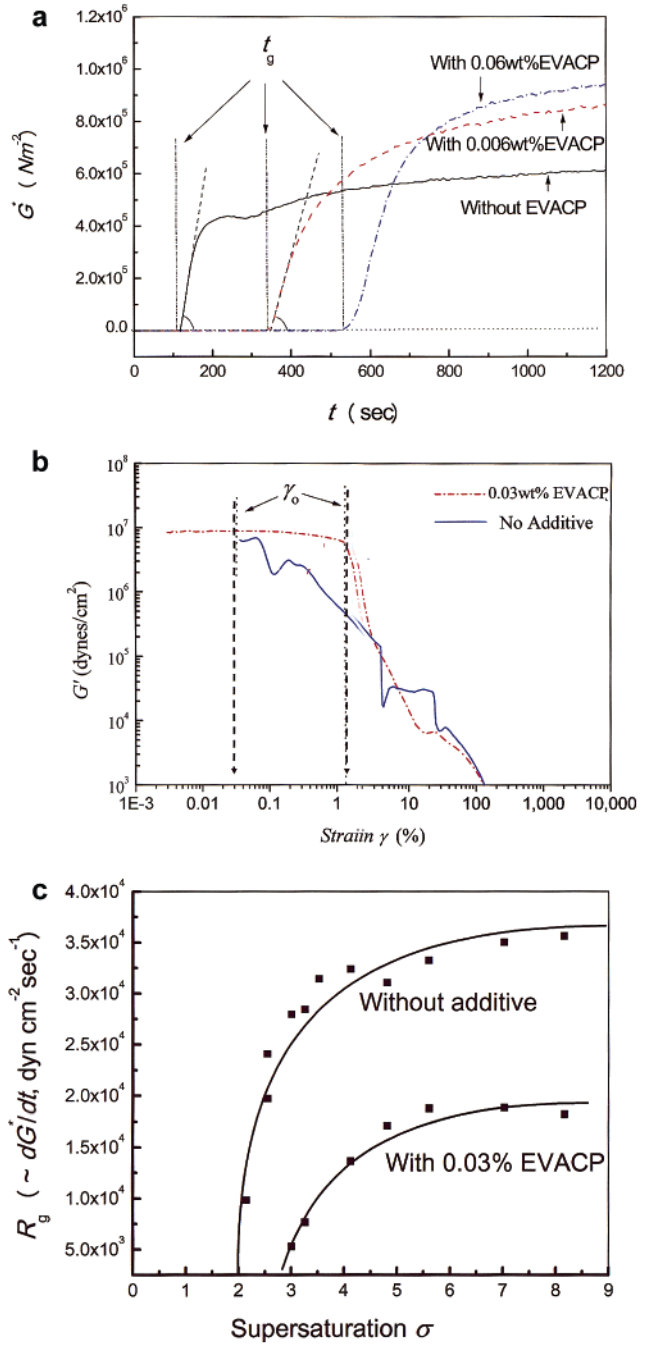

Figure 3. The changes of the rheological properties of the 10 wt % L-DHL/DIOP system in the absence and presence of EVACP as functions of time or strain. The rheological properties of the above system were measured by an advanced rheological expansion system. (This advanced rheometer allows us to control the temperature from 600.0 to −150.0 ± 0.1 °C.) (a) Dependence of the complex modulus G^* on time. The maximal G^* is almost doubled after adding EVACP. (b) Dependence of the storage modulus G^* on strain. The linearity limit γ_o is enhanced almost 100 times after adding EVACP. (c) R_g ($\sim$dG^*/dt) vs supersaturation σ for 10% lanosterol-DIOP without and with EVACP.

networks is the branching process at the growing tips of nanofibers (cf. Figure 5b), which can be understood as follows. The formation of sharp crystalline needles or fibers can be regarded as the result of the rapid growth of the tips.[13,15] This implies that in comparison with other directions, the kinetic resistance in the direction of the sharp fiber tips is very low because of the very low step free energy (the energy required to create a step at the crystal surface).[15] The growth of the fibers

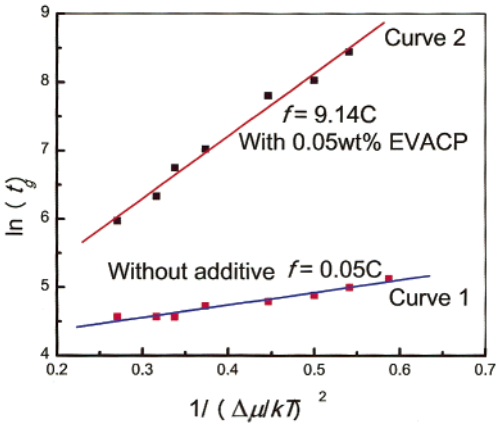

Figure 4. ln $t_g \sim 1/(\Delta\mu/kT)^2$ plots for the systems in the absence and presence of EVACP (0.03 wt %). Both give rise to a linear relation, indicating the control of nucleation during the fiber formation.[13] The slope of the straight lines represents the specific f.[13] After introducing EVACP, f is raised by more than 183 times confirming the significant mismatch between the nucleating fibers and the substrate caused by the additive.

in the fibrous axis orientation implies the deposition of new crystal layers on the top of the existing layer, and the crystal structure of the newly created layers matches perfectly with that of the existing surface of fibers (see Figure 5a).[13,15,16]

On the other hand, for any crystallization system, there is a certain probability for mismatch nucleation in which the surface of existing fiber tips serves as a perfect substrate for self- or auto-epitaxial nucleation at relatively high supersaturations (cf. Figure 5b). The occurrence of the mismatch nucleation, leading to the occurrence of new fiber branches (cf. Figure 5b), depends on both the structural match between the substrate and the nucleating phase and on supersaturation.[13,16] For the growth of L-DHL needles, the deposition of new layers on the existing surface of growing tips requires a perfect structural match, which occurs at very low surface supersaturations[13,15] (Figure 5a). Since EVACP is an agent that will selectively adsorb on certain surfaces of organic crystals,[17] the adsorbed molecules will disrupt structural match between new layers and the tip surface of parent fibers. Such the adsorption and the hindering of the normal growth of fibers can be examined from the slope of $G^* \sim t(=\mathrm{d}G'/\mathrm{d}t)$ at $t \rightarrow t_g$ ($t > t_g$).

The slope of $G^* \sim t$ (=dG'/dt) at $t \rightarrow t_g$ ($t > t_g$) (cf. Figure 3a) represents the growth rate of the L-DHL fibers. According to Einstein's relation,[7] the specific viscosity η_{sp} can be related to the volume fraction of the L-DHL needles as $\eta_{sp} \approx F\varphi$ with $\eta_{sp} = \eta^*/\eta_o - 1$, ($F$: shape factor of particle; η_o: viscosity of solvent, the complex viscosity $\eta^* = |G^*|/\omega$). The growth of L-DHL fibers can be regarded as the lengthening of the fibers in their axial directions since the area of crossing section remains almost constant. It follows that $\mathrm{d}\eta_{sp}/\mathrm{d}t = (1/\eta_0)(\mathrm{d}\eta^*/\mathrm{d}t) = (1/\eta_0\omega)(\mathrm{d}G^*/\mathrm{d}t)$ and $(\mathrm{d}\eta_{sp}/\mathrm{d}t) = (F/\eta_0)(\mathrm{d}\varphi/\mathrm{d}t) = (F/\eta_0)$-$(\mathrm{d}/\mathrm{d}t)(N_{fib}v_{fib}/V) \approx (FN_{fib}/\eta_0 V)(\mathrm{d}v_{fib}/\mathrm{d}t) = (FN_{fib}\phi/\eta_0 V)(\mathrm{d}L/\mathrm{d}t)$, where V is the total volume of crystalline materials at $t \rightarrow \infty$, N_{fib} is the number of fibers, v_{fib} is the average volume of fibers, and L denotes the length of the fibers. Combining the above two equations yields $\mathrm{d}G^*/\mathrm{d} \propto \mathrm{d}L/\mathrm{d}t = R_g$ (R_g: the growth

(16) Strom, C. S.; Liu, X. Y.; Wang, M. *J. Phys. Chem.* **2000**, *B104*, 9638−9646. Liu, X. Y.; Strom, C. S. *Chem. J. Phys.* **2000**, *112*, 4408−4411.
(17) Bennema, P.; Liu, X. Y.; Lewtas, K.; Tack, R. D.; Rijpkema, J. J. M.; Robers, K. J. *J. Cryst. Growth* **1992**, *121*, 679.

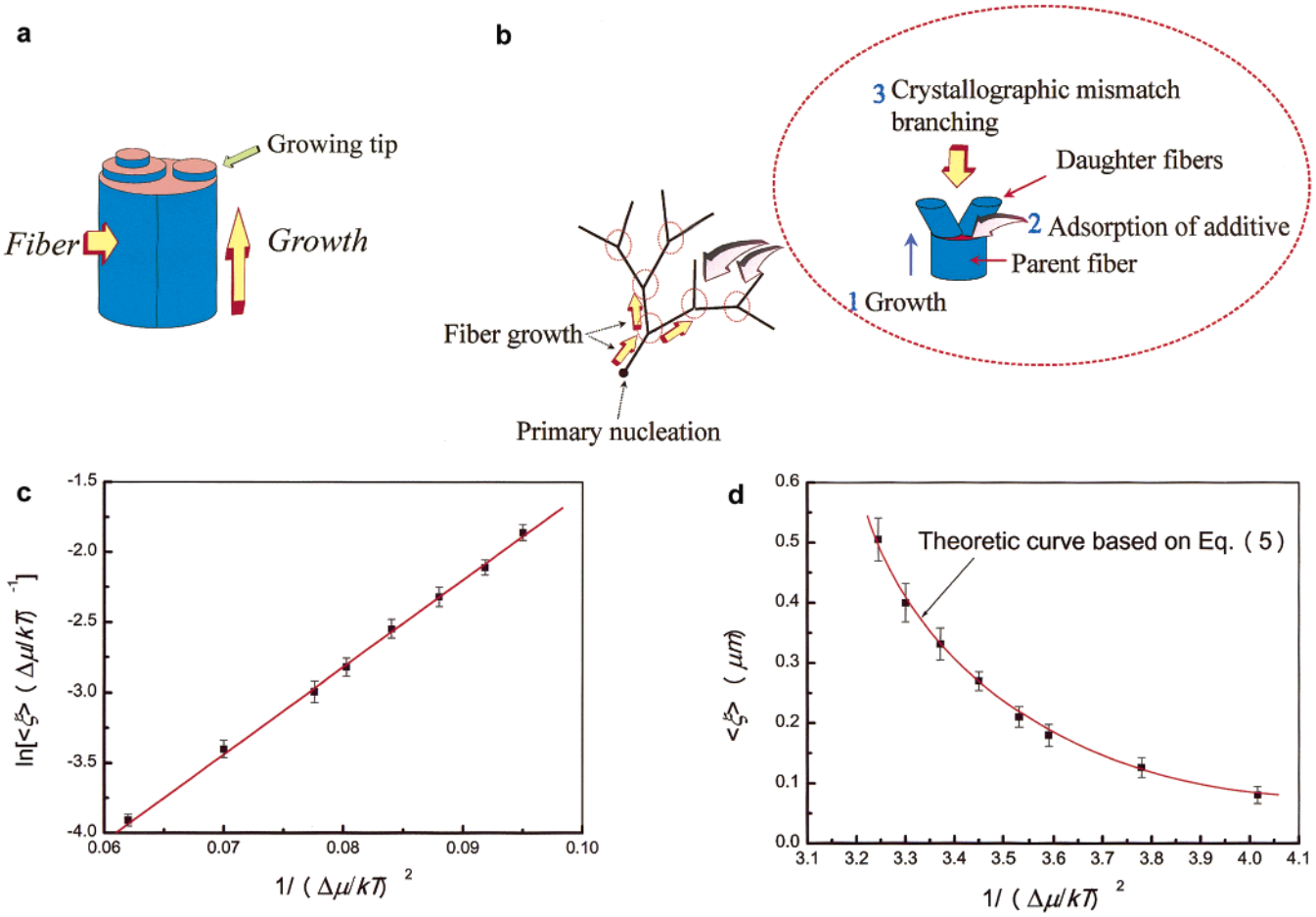

Figure 5. (a) The growth of the L-DHL fiber by depositing new crystal layers on the existing crystal surface.[17,18] This process can take place at low supersaturations, and consequently the structure of the new layers occurring at the tip of the fibers matches exactly that of the crystal surface. (b) The adsorption of EVACP causes mismatch nucleation at the tip of the growing fiber leading to crystallographic mismatch branching. The formation of interconnecting fiber networks via the process of primary nucleation−growth−branching−growth−branching−.... (c) The correlation between $\ln[\langle\xi\rangle(\Delta\mu/kT)^{-1}]$ and $1/(\Delta\mu/kT)^2$ for a L-DHL/DIOP system with 0.01% EVACP at $T = 20$ °C. The linear relationship confirms the governing role of the crystallographic mismatch branching mechanism in the formation of organized interconnecting fiber networks. (d) Dependence of the average branching distance on supersaturation for the same system. $T = 298.15$ K, $X = 0.026$. Supersaturation difference $\Delta\mu/kT$ is obtained by changing the molar fraction of solute in the solutions (cf. eq 2).

rate of fiber tips). This means that the slope of the straight lines in Figure 3a denotes the growth rate of the fibers.

Figure 3c shows the growth rate of L-DHL fiber tips R_g as a function of supersaturation σ (10 wt % L-DHL in DIOP solutions without additive and with 0.05 wt % EVACP). The results can be summarized as follows: (1) the growth rate of L-DHL fibers increases drastically with the supersaturation at the beginning, then gradually levels off as supersaturation increases further. Since supersaturation is very high, the growth kinetics at the high supersaturation regimes is governed by the diffusion of growth units in the viscous medium.[16] Nevertheless, how to describe the kinetics of this type requires more efforts and further attention. (2) The introduction of EVACP causes a reduction in the growth rate of L-DHL fibers (only 1/2 in comparison with that in the solution without EVACP) Since the addition of EVACP is only a tiny amount, the mutual diffusivity may not be changed much. Therefore, the growth rate reduction is due to the adsorption on the growth tips of the fibers, which slows down the surface kinetics of the tip growth.[13,15]

The structure mismatch caused by the adsorption of EVACP can be verified by the enhancement of f in heterogeneous nucleation experiments. The structural match between the newly created crystal layers and the tip surface can be described by f (and f') ($0 < f, f'' \leq 1$) in eq 1 (and eq 5 given later). According to the heterogeneous nucleation models,[13] the slope of the $\ln(t_g) \sim 1/(\Delta\mu/kT)^2$ plot corresponds to the specific f.[13] In a perfect structural match (such as crystal growth), one has $f, f = 0$, while for completely structural mismatch, one has $f, f' = 1$.[13] If the adsorption of EVACP on any substrate (including the tips of growing fibers) is capable of disrupting the structural match, one should observe a significant enhencement of f in the nucleation experiments.[13] Figure 4 shows that f indeed is raised by a factor of more than 183 after introducing EVACP, which confirms the significant structural mismatch caused by the adsorption of EVACP.

Since EVACP molecules can strongly adsorb on the tip of growing fibers and disrupt structural match between new layers and the tip surface of parent fibers (cf. Figure 5a), the structural match between the parent fibers and the new fiber layers will be disturbed (cf. Figure 5b). This then leads to the branching of fibers, which is called *crystallographic mismatch branching* (CMB) hereafter (Figure 5b).

On the basis of the above analysis and Figure 2b, the interconnecting network formation can he regarded as follows: *primary nucleation*−growth−CMB−growth− CMB... (cf. Fig-

ure 5b). Our latest results indicate that the formation of interconnecting the 3D networks or agarose and organic gels is actually controlled by this mechanism (work in progress).

To verify quantitatively the above mechanism, we will examine the correlation between the average branching distance $\langle\xi\rangle$ and supersaturation. In practice, crystallographic mismatch nucleation and the growth of fibers can be approximately regarded as two independent physical processes. Given that the induction time for the nucleation of new fibers on the host fibers is τ ($\tau \approx 1/J$; J: the rate of the crystallographic mismatch nucleation) and that the growth rate of fibers in the fibril axis direction is R_g, it follows then that the average branching distance can be expressed as

$$\langle\xi\rangle \sim R_{g\tau} \sim R_g/J \tag{3}$$

Referring to Figure 2a, the surfaces of L-DHL fiber tips are in principle rounded; the growth of L-DHL fibers is therefore very likely controlled by the so-called roughened growth mechanisms,[13,15] which gives rise to the growth rate[15]

$$R_g = C_1\left(\frac{\Delta\mu}{kT}\right) \tag{4}$$

where C_1 is a coefficient associated with volume transport and should be a constant for a given condition.[15,18] Adopting eqs 1 and 4, the average branching distance $\langle\xi\rangle$ of crystallographic mismatch branching, which determines the average mesh size, can be given as

$$\langle\xi\rangle = C_2\frac{(\Delta\mu/kT)}{f'f^{1/2}}\exp\left\{\frac{16\pi f}{3(\Delta\mu/kT)^2}\left(\frac{\gamma_{cf}\Omega^{2/3}}{kT}\right)^3\right\} \tag{5}$$

where $C_2 = C_1/B$. The average length $\langle\xi\rangle$ of the branches, which is proportional to the mesh size in the fiber networks, was examined by SEM. The linear relation between $\ln[\langle\xi\rangle(\Delta\mu/kT)^{-1}]$ and $1/(\Delta\mu/kT)^2$ obtained for the aforementioned L-DHL/DIOP system with 0.03% EVACP (see Figure 5c) verifies the above branching mechanism described by eq 5.

The branching promotion by EVACP can be quantitatively understood as follows. According to eq 5, a perfect structural match between the parent fibers and the newly created crystal layers ($f \approx 0$, cf. Figure 4) will give rise to an infinite $\langle\xi\rangle$, meaning that fiber growth occurs without branching. To obtain a finite branch distance, a high degree of structural mismatch (a large nonzero f) is required. As shown by Figure 4, the addition of EVACP results in a drastic increase of f for almost 183 times. This is the reason that CMB is promoted after addition of EVACP.

The addition of EVACP leads to much thinner L-DHL fibers (cf. Figure 2a and b). The thinning of L-DHL fibers means that the ratio between the growth rate of the fibers and that of the tips increases after the addition of EVACP. This implies that EVACP will not only adsorb on the tips but also on the prism face of L-DHL fibers.[15] Notice that the CMB can also occur in the prism faces of L-DHL fibers. Nevertheless, if the tip branch condition can be fulfilled, CMB will occur first at the tips of fibers since the tips are the rapid growth direction and will first grow into highly supersaturated bulk solutions.[15]

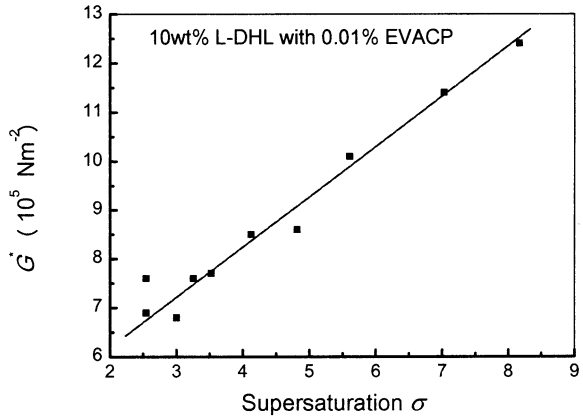

Figure 6. Dependence of G^* on supersaturation σ for the 10 wt % L-DHL in DIOP with 0.01% EVACP.

Engineering of 3D Interlinking Nanofiber Network and Rheological Properties of Functional Materials. As illustrated by Figure 1a and 1b, one aspect of the engineering of supramolecular functional materials is the architecture of self-organized 3D interconnecting nanofiber structure (Figure 1a), and the other aspect is to tune the micro- or nanostructure in a predictive way (Figure 1b). It has been shown in the previous sections that the variations in the micro- or nanostructure of functional materials will exert direct impact on the rheological or other physical properties. This implies that it is possible to control the mesh size and the corresponding fiber network structure so as to obtain functional materials with the desired micro- or nanostructure and rheological properties. In other words, the materials with required properties can be obtained by altering the experimental conditions.

Figure 5d shows the dependence of $\langle\xi\rangle$ on the supersaturation, meaning that the micro- or nanostructure can be modified by changing supersaturation according to eq 5. The decrease of the mesh size of the 3D interconnecting networks of the materials will lead to the increase of G^*, G', and so forth.[14] Therefore, the change of supersaturation should enable us to alter the rheological or other physical properties of the materials. Figure 6a shows the dependence of G^* on supersaturation for the system given in Figure 5d and e (10 wt % L-DHL in DIOP with 0.01% EVACP). As expected, G^* increases with supersaturation (see Figure 6).

Under the identical conditions, the increase of the concentration of branching promoter (additive) will also cause the reduction of the mesh size of 3D interconnecting networks of the materials in terms of further branching promotion. Figure 7a and b shows the 3D fiber network structures of L-DHL in 10 wt % L-DHL/DIOP gels with 0.01 wt % and 0.1 wt % EVACP, respectively. Raising EVACP concentration C_{EVACP} causes the reduction of the mesh size of the networks. This consequently will give rise to the increase of G^*, G', and so forth (cf. Figure 7c).

From the technological point of view, highly porous and self-supporting monolithic foams, which have many important applications including novel bioseparation,[19] can be obtained from the above materials after applying the CO_2 supercritical extraction (cf. Figure 2b). In addition, organic nanofiber

(18) Liu, X. Y.; Maiwa, K.; Tsukamoto, K. *J. Chem. Phys.* **1997**, *106*, 1870.

(19) Shi, C.; Huang, Z.; Kilic, S.; Xu, J.; Enick, R. M.; Beckman, E. J.; Carr, A. J.; Melendez, R. E.; Hamilton, A. D. *Science* **1999**, *286*, 1540−1543.

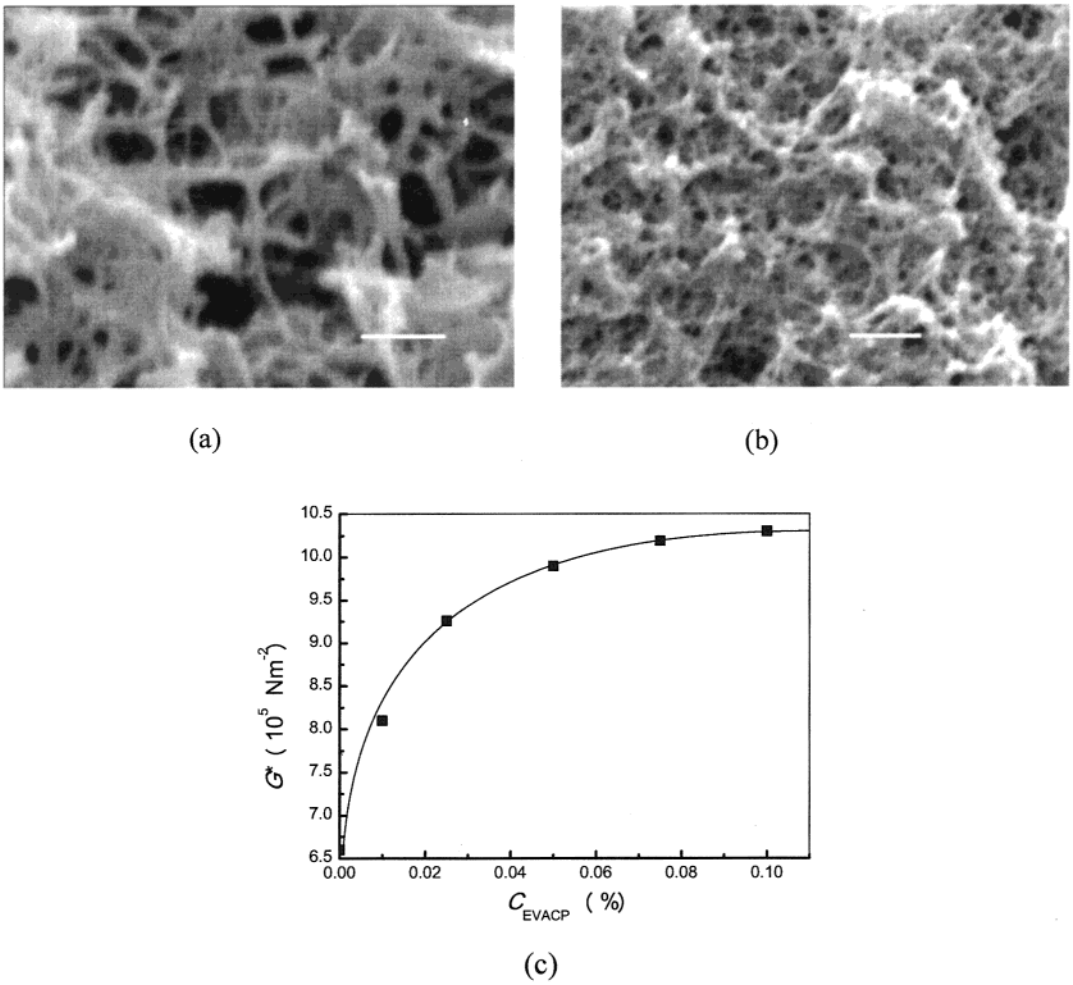

Figure 7. Effects of EVACP concentration on the micro- or nanofiber structure and rheological properties of L-DHL. The increase of EVACP concentration C_{EVACP} will give rise to the reduction of the mesh size of L-DHL network (cf. a and b) and the rise of G^*. (a) Fiber network of L-DHL obtained from 10 wt % L-DHL in DIOP with 0.01 wt % EVACP. (b) Fiber network of L-DHL obtained from 10 wt % L-DHL in DIOP with 0.1 wt % EVACP. (c) Dependence of G^* on C_{EVACP} (10 wt % L-DHL in DIOP).

networks can be used as a template for the preparation of nanostructured materials by the gel-template-leading process.[20−22] The network can be created and controlled on the basis of the above approaches. We should be able to engineer directly the microstructure and macroscopic properties of the above materials in a controlled manner.

Principles and Strategies for the Design and Selection of Branching Promoter. To promote branching at fibers, branching promoters (or additives) should be adsorbed effectively on the growing tips to disrupt and hinder the normal growth of the fibers in the axial orientations. One of the key questions to be addressed is how to design or select branching promoters. In the following discussion, we will provide such guidelines from the molecular structural point of view, on the basis of the results obtained from consistent-field theory calculations.[23−26] The branching promoter molecules should possess the following characteristics:

(1) Large molecule with a relatively rigid basic structure. For different molecules of similar types, larger molecules with somewhat rigid structures are easily adsorbed at interfaces.[23,24] This criterion is based on both energetic and entropic consideration.

Energy Consideration. Given that there is a strong interaction between each monomer and the crystal surface, polymers or macromolecules with the similar structural units as a whole have more interacting points with the crystal surface than single monomers. Therefore, the desorption of polymers are much more difficult.

Entropy Consideration. Our calculations[23−26] show that long and relatively rigid polymers have a much higher surface activity because of the entropy effect. There are two contradictional entropic effects in the adsorption polymers or macromolecules. The first effect is the so-called *free particle entropic effect*. Normally, there is a solvation layer around larger molecules or polymers and the crystal surface (see Figure 8a) where solvent molecules are semilocalized or bonded to the surfaces. If these additive molecules adsorb onto the crystal surface, these

(20) Beginn, U.; Keinath, S.; Mõller, M. *Macromol. Chem. Phys*. **1998**, *199*, 2379−2384.
(21) Gu, W.; Lu, L.; Chapman, G. B.; Weiss, R. G. *Chem. Commun.* **1999**, 543−544.
(22) Hafkamp, R. J.; Kokke, B. P. A.; Danke, I. M.; Geurts, H. R. M.; Rowan, A. F.; Feiters, M. C.; Nolte, K. J. M. *Chem. Commun.* **1997**, 545−546.
(23) Liu, X. Y.; Bennema, P. *Phys. Rev. E* **1993**, *48*, 2006. Liu, X. Y. *Phys. Rev. E* **1994**, *49*, 583.
(24) Liu, X. Y.; Bennema, P.; Meijer, C.; Couto, M. *Chem. Phys. Lett.* **1994**, *220*, 53.
(25) Liu, X. Y. *Phys. Rev. B* **1999**, *60*, 2810; *J. Chem. Phys.* **1995**, *102*, 1373−1384.
(26) Liu, X. Y. *J. Cryst. Growth* **1997**, *174*, 280−385.

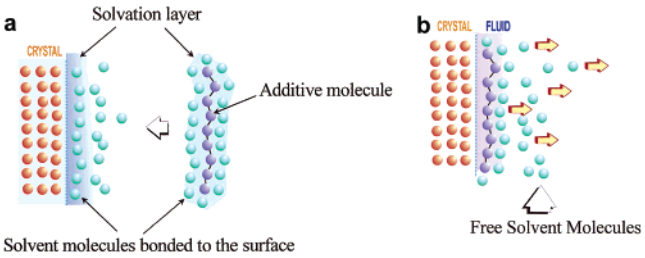

Figure 8. Illustration of the adsorption of additive molecules onto the crystal surface. (a) Solvent molecules are partially bonded to the surfaces of additive molecule and crystals. (b) The adsorption of additive molecule to the surface of crystal will release semibonded solvent molecules, leading to the increase of entropy.

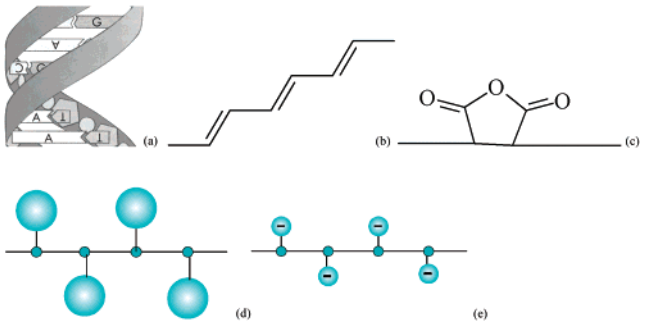

Figure 9. Rigidity of molecules because of (a) intramolecule hydrogen bond, (b) double covalent bond, (c) rigid ring structure, (d) neighboring bulky branch (hindered rotation), and (e) electric repulsion (hindered rotation).

semibonded solvent molecules will be liberated from the surfaces of additive molecules and the crystal surface, resulting in the increase of entropy. According to the definition of entropy,[27] the increase of free particle entropy (per molecule) is proportional to $k \ln(2N_{surf})$ (k: Boltzmann const; N_{surf}: the number of monomers or atoms on the surface of macromolecule). Therefore, larger or longer molecules, such as polymers or macromolecules, will result in a large entropy increase if they are adsorbed onto the surface. This is why most effective tailormade additives are either long polymers or macromolecules.

On the other hand, polymers or macromolecules have a very high conformational entropy, depending on the number of atoms or monomers in a polymer or a macromolecule and the degree of internal motion freedom. This is so-called conformational entropic effect.[27] For molecules with the maximal degree of freedom of internal motion (such as polymers with completely flexible chains), the conformational entropy is proportional to $k \ln(3N)$, whereas molecules with no internal motion freedom (such as polymers with completely rigid chains) have a conformational entropy of $k \ln 6$ ($k \ln 5$ for linear molecules).[27] When additive molecules are adsorbed onto the crystal surface, the internal motion of the molecules is to a large extent frozen. This implies that when polymers or macromolecules are adsorbed onto the crystal surface, they will lose the conformational entropy from $k \ln 5$ (completely rigid molecules) up to $k \ln(3N)$ (completely flexible molecules), depending on the rigidity of molecules. Therefore, conformational entropy is in contradiction to the free particle entropy.

Combining these two contradiction effects together, one will have for linear or flat molecules ($N_{surf} = N$) the entropy increase (per molecule) due to adsorption $\approx k \ln(2/3)$ for completely flexible molecules and $k \ln(2N/5)$ for completely rigid linear molecules. In other words, the adsorption of completely flexible molecules on the crystal surface will lose the entropy due to the restriction of molecular internal movement. This will consequently give rise to the depletion of the molecules at the surface. One the other hand, the adsorption of completely rigid molecules will gain entropy since the loss of chain conformation entropy is very limited in this process. This will consequently result in the strong adsorption of the molecules. This trend is further enhanced as the number of monomers or atoms in additive molecule increases. Normally, the semirigid chain will be between the above two extremes. These results have been confirmed by our SCF calculations.[23−25]

Note that the length of polymers cannot be extended without limitation. Molecules with chains too long tend to fold and lose much chain conformational entropy in the adsorption. Normally, the relative rigidity of a molecule decreases with its size. For a given type of relatively rigid molecule, the increase of the entropy in adsorption will reach its maximum at a certain N.

The rigidity of additive molecules can result from a variety of reasons. In the following, we will summarize some typical examples where rigid molecules can be obtained.

(i) Intramolecular Bonding. Molecules will become relatively rigid if some intramolecular bonds, such as hydrogen bonds (Figure 9a), double or triple covalent bonds (Figure 9b), rigid rings (Figure 9c), and so forth, occur in the backbone of additive molecules.

(ii) Hindered Rotation. The folding of chainlike molecules is in many cases attributed to the rotation around single carbon−carbon bonds. Bulky functional groups attached to the neighboring units in polymers or macromolecules will cause them to avoid each other because of the steric repulsion (Figure 9d). For polyelectrolyte, the groups with the same charges attaching to the backbone of additive molecules will avoid each other because of electric repulsion (Figure 9e). These will hinder the chain rotation, leading to more stiff or rigid chains.

Notice that the additives (branching promoters) need not to be linear polymers. It can be any type or shape of large molecules or macromolecules as long as the above criteria are satisfied.

(2) Stronger interaction between additives and the crystal surface will lead to a stronger adsorption at the surface.[23−26] Since the surface of crystals is highly ordered and stiff, in order to obtain the maximal interactions by matching the structure of the crystal surface, it is desirable to have short and relatively flexible functional groups attached to the backbone of additive molecules so that they can adjust their positions to obtain optimal interactions with the solid molecules at the surface of crystals. Normally, some function groups or branches attached to the backbones of additives are designed to have a molecular structure similar to that of solid molecules of the crystals, or strong interactions with the solid molecules at the crystal surface. This is to strengthen interactions between additives and the crystal surface.

(3) The adsorbed additives should interrupt the growth of crystal layers along the crystal surface.[23−26] The repulsions can originate from steric, electrostatic, polar/nonpolar, or hydro-

(27) Fowler, R.; Guggenhein, E. A. *Statistic Thermodynamics*; Cambridge University Press: London, 1960.

philic/hydrophobic forces and can be achieved by attaching some functional groups to the backbone of additives.

(4) The concentration of additives also plays a certain role. For a given system, the excess in the concentration may not enhance the adsorption; it sometimes can even cause a decrease in the adsorption.[23−26] This is attributed to the adsorption synergism by mixing additives with other structural units. Note that all above-mentioned factors are correlated to each other. Therefore, these factors should be considered from different aspects.

EVACP has the molecular structure as follows:

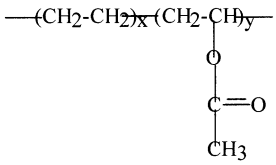

Obviously, the structure satisfies all the structural requirements for branching promoters: $(C_4H_6O_2)_x$ in the molecules fulfills (1) and (2) (cf. Figure 9d) and $(C_2H_4)_y$ satisfies the requirement of (3). This is why EVACP can become an effective branching promoter. Poly(vinyl chloride) (PVC, MW: 100000, from BDH, U.K.) has the molecular structure as follows

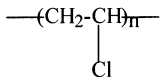

Although PVC is a polymer with the polyethylene backbone (similar to EVACP), the molecules do not satisfy the rigidity and the other criteria ((2) and (3)). Therefore, PVC has no effect in promoting the branching in L-DHL and therefore cannot serve as a branching promoter. This is verified by our experiments.

In conclusion, we have identified a completely new approach to produce new supramolecular functional materials in terms of micro- or nanostructure architecture. This architecture in the micro- or nanoscale is based on the crystallographic mismatch branching and is achieved by branching promoters. Furthermore, the micro- or nanostructure of the materials can be tuned by either altering the supersaturation of solutions or changing the concentration of branching promoters. The effective branching promoters should strongly adsorb onto the tips and disrupt the regular growth of growing fibers.

JA0206137